Nanocrystalline BaCo 3 (VO 4) 2 (OH) 2 with a kagome lattice of Co(ii) ions: synthesis, crystal structure and magnetic properties

R. Dessapt, L. Lajaunie, J. Calvino, P. Deniard, I. Trenque, C. Payen

COMMUNICATION

Nanocrystalline $BaCo_3(VO_4)_2(OH)_2$ with a kagome lattice of Co(II) ions: synthesis, crystal structure and magnetic properties

Received 00th January 20xx,
Accepted 00th January 20xx

DOI: 10.1039/x0xx00000x

R. Dessapt,*[a] L. Lajaunie, [b,c] J. J. Calvino,[b,c] P. Deniard,[a] I. Trenque [a] and C. Payen*[,a]

We report an initial magnetic study of highly crystalline nanoparticles of the layered-kagome compound $BaCo_3(VO_4)_2(OH)_2$. Quasi-spherical nanoparticles with size in the range of 9-25 nm were elaborated for the first time via a new synthetic route at ambient pressure. Rietveld refinement of X-ray diffraction data, vibrational spectrocopies and high-resolution scanning transmission electron microscopy indicates that the rhombohedral crystal structure of $BaCo_3(VO_4)_2(OH)_2$ is not modified by nanostructuring. Magnetisation measurements are consistent with high-spin Co^{2+} ions for which unquenched orbital angular momentum is present. Temperature-dependent magnetic susceptibility shows no apparent magnetic ordering or spin freezing down to 2 K and suggests finite-size or surface effects at low temperatures.

Introduction

Materials based on 3d transition metal (TM) ions with triangular, honeycomb or kagome lattices are interesting candidates for studying geometric frustration and spin liquids,[1,2] 2D ferromagnetism,[3] layered multiferroics[4] or even Kitaev interactions.[5] Recent technological opportunities have also arisen in the field of spintronic.[6] While fundamental research ideally requires single-crystals, considering potential applications implies other material forms, including nanostructuration,[7] and many initially studies of new materials are undertaken on polycrystalline samples. Therefore, synthetizing and studying new materials with 2D lattices of TM ions in various forms (bulk, nano and thin film) is of great interest. In particular, high-spin d^7 materials are currently actively investigated as new quantum magnets with spin-orbit coupling (SOC).[5,8,9] In this context, we targeted the Co^{2+} orthovanadate $BaCo_3(VO_4)_2(OH)_2$ because its magnetic properties remain unexplored.[10] Its layered rhombohedral crystal structure (*R*-3*m* space group) is similar but not identical to those of the copper mineral vesignieite $BaCu_3(VO_4)_2(OH)_2$ (monoclinic, *C2/m* space group),[11,12] which is a well-known spin-1/2 kagome antiferromagnet, and of the spin-1 nickel compound $BaNi_3(VO_4)_2(OH)_2$ (monoclinic, *C2/m* space group),[13] which exhibits a glassy magnetic transition at low temperature. Very small single-crystals of $BaCo_3(VO_4)_2(OH)_2$ were already obtained with moderate yield (ca 35%), together with an uninvestigated powder, by hydrothermal reaction.[10] Their crystal structure comprises regular 2D kagome planes of edge-sharing CoO_6 octahedra. However, the size and the quality of these single-crystals did not permit measurements of the physical properties. Here, we present a new soft-chemistry route to quantitatively obtain phase-pure samples of $BaCo_3(VO_4)_2(OH)_2$ consisting of highly crystalline quasi-spherical nanoparticles (NPs). $BaCo_3(VO_4)_2(OH)_2$ NPs have been characterized using powder X-ray diffraction (PXRD), FT-IR and FT-Raman spectroscopies, energy-dispersive X-ray spectroscopy (EDS), aberration-corrected high-resolution scanning transmission electron microscopy (HR-STEM) including image simulations, and magnetisation measurements.

Results and discussion

$BaCo_3(VO_4)_2(OH)_2$ NPs were prepared in a reproducible manner by using a simple coprecipitation method in ambient pressure. An aqueous solution (4 mL) of barium acetate $Ba(CH_3COO)_2$ (0.520 g - 2 mmol) was added slowly to an aqueous solution (32 mL) of $Co(NO_3)_2{\cdot}6H_2O$ (0.872 g - 3 mmol) and ammonium metavanadate NH_4VO_3 (0.234 g - 2 mmol) at 90°C under vigorous magnetic stirring, leading to immediate precipitation of a light brown solid. The pH was adjusted to 6 by

[a] *Université de Nantes, CNRS, Institut des Matériaux Jean Rouxel, IMN, F-44000 Nantes, France. E-mail: remi.dessapt@cnrs-imn.fr, christophe.payen@cnrs-imn.fr*
[b] *Departamento de Ciencia de los Materiales e Ingeniería Metalúrgica y Química Inorgánica, Facultad de Ciencias, Universidad de Cádiz, Campus Río San Pedro S/N, Puerto Real, 11510, Cádiz, Spain. E-mail: luc.lajaunie@uca.es*
[c] *Instituto Universitario de Investigación de Microscopía Electrónica y Materiales (IMEYMAT), Facultad de Ciencias, Universidad de Cádiz, Campus Río San Pedro S/N, Puerto Real 11510, Cádiz, Spain. E-mail: luc.lajaunie@uca.es*
Electronic Supplementary Information (ESI) available: Experimental section with structural parameters, FT-IR and FT-Raman spectra, Fragment of kagome layer, SEM image, EDS spectrum, χ.T product. See DOI: 10.1039/x0xx00000x

adding manually NH_3 6 M, and the slurry was stirred at 90°C for 3 hours. After filtration, the powder was washed with water and ethanol and dried in air at room temperature (96 % yield in Co). Noticeably, the as-prepared powder exhibits a high specific surface area of 61 m^2/g.

The purity and crystallinity of the sample were confirmed by PXRD analysis at room temperature, and the Rietveld refinement was performed using previously published structural model.[10] Fig. 1a shows the quality of the refinement. The final reliability factors under the *R*-3*m* space group (a = 5.9085(4) Å, c = 21.099(2) Å) are R_{wp} = 2.19 and Gof = 1.09. The computed crystallite sizes are 22.2(3) nm and 18.7(4) nm perpendicular and parallel to [001], respectively. Structural parameters are gathered in Table S1, ESI†. All refined parameters compare well with those previously obtained from single-crystals.[10]

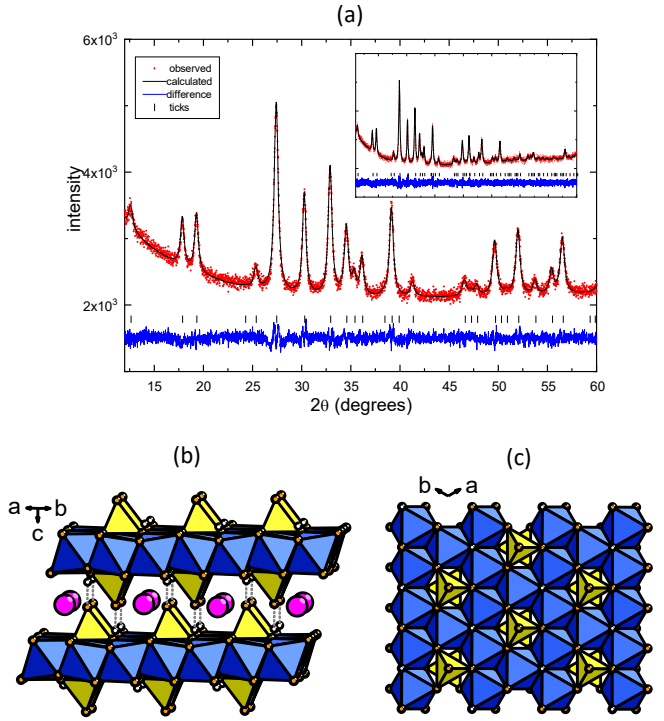

Fig. 1 (a) Rietveld refinement for $BaCo_3(VO_4)_2(OH)_2$ NPs showing observed, calculated and difference patterns with the total pattern as inset. The high-level noisy pattern is due to cobalt fluorescence. Structure of $BaCo_3(VO_4)_2(OH)_2$ viewed along the *c*-axis (b) and perpendicular to the *c*-axis (c). Blue octahedra: CoO_6, yellow tetrahedra: VO_4, orange sphere: oxygen, pink sphere: barium, white sphere: hydrogen. Hydrogen bonds are displayed as grey dotted lines.

The structure is built upon $\{Co_3(VO_4)_2(OH)_2\}^{2-}$ layers stacked along the *c*-axis and separated by 7.03 Å due to the presence of large Ba^{2+} ions between the layers (Fig. 1b). These layers are made up of edge-shared $CoO_4(OH)_2$ octahedra in which the Co^{2+} ions are coordinated to four equivalent equatorial oxo ligands (Co-O2 = 2.176(4) Å) and two shorter axial hydroxide ones (Co-O3 = 1.9407(6) Å). The Co^{2+} ions form a regular 2D kagome lattice (Fig. 1c and Fig. S2, ESI†), and the distance between two adjacent Co^{2+} ions is 2.954 Å. The orthovanadate VO_4^{3-} groups are located on both sides of the M^{2+} site deficiency of the kagome framework (Fig. 1c). Each slightly-distorted VO_4 tetrahedron belongs to the C_{3v} point group and connects the Co^{2+} ions via three equivalent O-atoms (V-O2 = 1.765(2) Å). The fourth V-O bond is shorter (V-O1 = 1.668(14) Å), and the O-atom is involved in strong hydrogen bonding interaction (O1···O3 distance of 2.60 Å) with the hydroxide ligand of a neighboring layer (Fig. 1b).

$BaCo_3(VO_4)_2(OH)_2$ NPs were also characterized by FT-IR and FT-Raman spectroscopies. Attribution of the vibration bands have been done by comparison with vibrational data of natural mineral $BaCu_3(VO_4)_2(OH)_2$ samples,[14] and other orthovanadate-containing materials.[15–17] The FT-IR spectrum of $BaCo_3(VO_4)_2(OH)_2$ NPs (Fig. S1a, ESI†) shows a weak band at 980 cm^{-1} and two intense ones at 908 and 756 cm^{-1} which are assigned to the stretching modes of VO_4^{3-} units with C_{3v} point group.[14] The band at 509 cm^{-1} may be assigned to a Co-O stretching mode. The two broad bands at 3425 and 2995 cm^{-1} characterize the νOH stretching modes, and the weak bands at 1852, 1635 and 1384 cm^{-1} are in direct line with combination and overtones modes.[17] In the FT-Raman spectrum of $BaCo_3(VO_4)_2(OH)_2$ NPs (Fig. S1b, ESI†), the bands at 885 and 790 cm^{-1} could be assigned to the ν_1 symmetric and ν_3 antisymmetric stretching modes of VO_4^{3-} units with C_{3v} point group.[14] The band at 472 cm^{-1} could be attributed to the ν_4 antisymmetric bending mode, while the more intense one at 327 cm^{-1} and that at 397 cm^{-1} could correspond to the ν_2 symmetric bending modes.

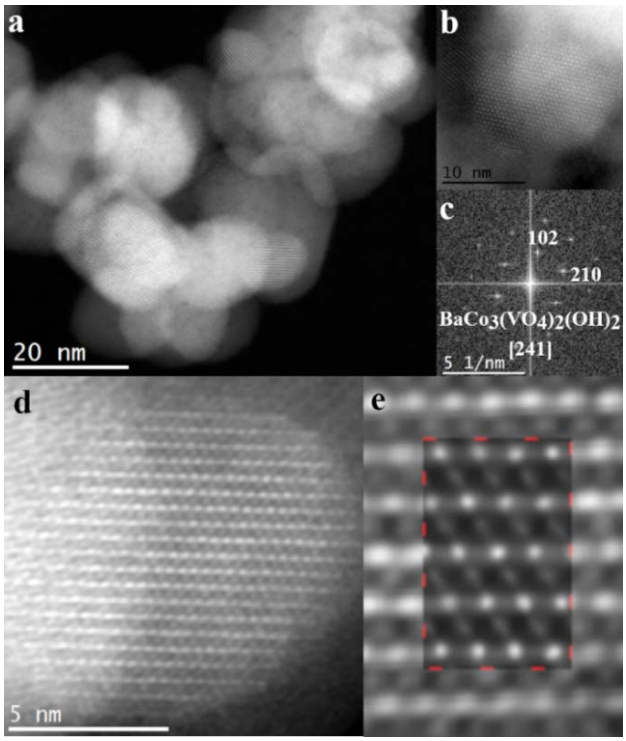

Fig. 2 Large view (a) and detail (b) HR-STEM HAADF micrographs of $BaCo_3(VO_4)_2(OH)_2$ NPs. (c) FFT pattern acquired on the nanoparticle shown in (b). It has been successfully indexed with the XRD-refined $BaCo_3(VO_4)_2(OH)_2$ structure seen along the [241] zone axis. (d) HR-STEM HAADF micrograph of a nanoparticle which is seen along the [-141] zone axis. (e) Superimposition of the experimental and simulated HR-STEM HAADF images. The experimental image is an enlargement of the

nanoparticle shown in (d). The simulated image is delimited by a red dashed line.

All NPs are quite homogeneous in shape and size, as shown by SEM analysis (Fig. S3, ESI†). Fig. 2 shows the HR-STEM HAADF analyses performed on the $BaCo_3(VO_4)_2(OH)_2$ NPs. They are quite regular in shape with a quasi-spherical morphology, and their diameter is between 9 and 25 nm. In agreement with PXRD results, this well evidences that each nanoparticle is a single crystallite. The high crystalline quality of the NPs can be clearly appreciated in the micrographs (Fig. 2a and 2b) and in the corresponding FFT pattern (Fig. 2c). In addition, the FFT pattern was successfully ascribed to the crystal structure of $BaCo_3(VO_4)_2(OH)_2$. The crystallographic structure of the nanoparticles was also confirmed by the excellent agreement between the experimental and simulated HR-STEM HAADF images (Fig. 2d and 2e). It should be noted that image simulations and FFT indexations were performed by using the PXRD-refined data as input. The Ba/Co, Ba/V and Co/V elemental ratios were determined by STEM-EDS analyses (Fig. S4, ESI†) and are equal to 0.33, 0.46 and 1.40, respectively. These values are in good agreement with the expected ones (0.33, 0.50 and 1.50, respectively). These findings confirm the results obtained from PXRD analysis regarding the crystallographic structure.

Then, the magnetic properties of the $BaCo_3(VO_4)_2(OH)_2$ NPs were studied using a commercial SQUID magnetometer. The temperature dependence of the inverse dc magnetic susceptibility, $1/\chi(T)$, is presented in Fig. 3. Data display Curie-Weiss behaviour, $\chi = C/(T-\theta)$ above ≈ 150 K. Its fitting from 150 K to 300 K yields C ≈ 0.01432 cm^3 K mol^{-1} and θ ≈ - 22 K. Using the molar weight of bulk $BaCo_3(VO_4)_2(OH)_2$, the fitted C value corresponds to an effective magnetic moment of 4.7 μ_B/Co atom, consistent with high-spin Co^{2+} (d^7, three unpaired electrons) ions for which unquenched orbital angular momentum is present.[18] For 3d TM ions having orbitally nondegenerate ground term, experimental magnetic moments are often close to the spin-only values and a negative θ implies dominant antiferromagnetic (AF) interactions. However, for high-spin Co^{2+} ions in a weak octahedral crystal field, the θ value determined from high-temperature susceptibility data could differ from the Weiss temperature of the molecular field approximation due to orbital degeneracy and SOC.[18] Below ≈ 100 K, a negative deviation of $1/\chi$ from the high-temperature Curie-Weiss behaviour is observed. In parallel, the $\chi(T).T$ product, shown in Fig. S5, ESI†, decreases less rapidly than required by the Curie-Weiss law when decreasing temperature in the range of 150-10 K. Similar deviation from the high-temperature Curie-Weiss behaviour was reported in other octahedral high-spin Co^{2+} bulk oxides, and was ascribed to the splitting between a Kramers doublet ground state with effective spin J_{eff} = ½ and lowest excited states.[19,20]

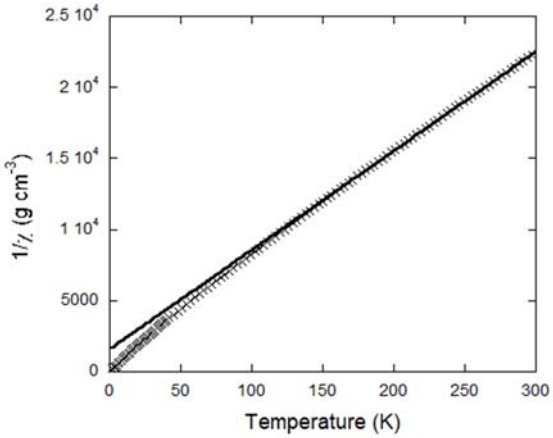

Fig. 3 Inverse magnetic susceptibility $1/\chi$ versus temperature T for $BaCo_3(VO_4)_2(OH)_2$ NPs. Data were acquired at a dc applied field of 5 kOe. The solid line corresponds to a Curie-Weiss behaviour, $1/\chi = (T-\theta)/C$, obtained from a fit to the data in the temperature range of 150-300 K.

As can be seen in Fig. 4, the dc magnetic susceptibility measured at a small applied field of 100 Oe keeps on rising down to 2 K with no difference between zero-field-cooled (ZFC) and field-cooled (FC) traces. There is no maximum in the $\chi(T).T$ versus T curve, too (Fig. S5, ESI†). These features, which have been observed for two independently prepared samples, would indicate the absence of magnetic ordering or spin freezing above 2K for a micrometer-sized sample. Below 10 K, both $\chi(T)$ and the $\chi(T).T$ product sharply increase with decreasing temperature. A log-log plot of $\chi(T)$ versus T shows that, in the vicinity of 10 K, there is a crossover from the sub-Curie high-temperature region to a weakly sample-dependent low temperature regime where $\chi(T)$ varies as $T^{-\alpha}$ with α = 2.1-2.4 (Fig. S6, ESI†). Magnetic field dependences of magnetization M(H) measured at temperatures between 2 and 50 K are shown in Fig. 4. At 50 K, only the anticipated linear paramagnetic response is observed. Below 10 K, the isothermal magnetization rapidly increases to 4-5 T and then linearly increases. As shown in Fig. S7, ESI†, isothermal magnetization data below 10 K do not follow the Brillouin H/T scaling for noninteracting spins, in agreement with the absence of a plateau in the $\chi(T).T$ vs T curve below 10 K. Fig. S8, ESI† shows that the M(H) data at 2 K are significantly different from Brillouin equations calculated for J = 3/2 with g = 2 and for an effective J = 1/2 with g = 4, which is a typical value observed in compounds containing high-spin Co^{2+} ion in a distorted octahedral environment.[8,19,21,22] Also, the value g = 4 is consistent with the theoretical expression for the g factor that can be calculated within the effective J_{eff} = 1/2 approach.[23] The magnetization versus field variation is not saturated even at 2 K and 7 T. The maximum value of the magnetization at 2 K (40 emu/g) corresponds to 1.4 μ_B/Co-atom, which is lower than the saturation values observed in bulk oxides or orthovanadate compounds containing high-spin Co^{2+} ions in octahedral environment.[8,9,21,22,24,25] The slope of the isothermal M(H) scan at high field (H > 4 T) and low temperature (T < 5 K) is at least four times higher than the Van Vleck paramagnetic susceptibility observed in high-spin Co^{2+} compounds,[21,22] suggesting the presence of AF interactions

and/or of magnetic anisotropy. Octahedral high-spin Co^{2+} moments are often anisotropic due to spin-orbit coupling.

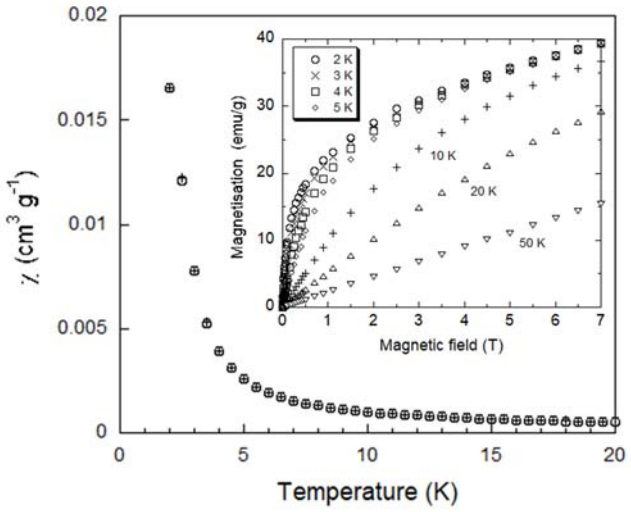

Fig. 4 Magnetic susceptibility χ versus temperature for $BaCo_3(VO_4)_2(OH)_2$ NPs at low temperatures. Data were collected at dc applied magnetic fields of 100 Oe under ZFC (open circles) and FC conditions (plus signs). Inset: magnetic field dependence of magnetisation measured at 2, 3, 4, 5, 10, 20, and 50 K.

The magnetic behaviour of $BaCo_3(VO_4)_2(OH)_2$ NPs cannot be fully explained at this initial stage. The fine-structure splitting of the lowest levels of the Co^{2+} ion under the action of crystal field, spin orbit-interaction, and magnetic field is unknown. The crystal structure contains compressed $CoO_4(OH)_2$ octahedra with four long equatorial Co-O2 distances and two short axial Co-O3 distances, but the actual local symmetry of the metal cation is lower than D_{4h} (all the O-Co-O angles differ from 90°). For a D_{4h} compression, the $^4T_{1g}$ ($t^5_{2g}e^2_g$, L = 1) state of the regular CoO_6 octahedra is split into a ^4E_g ($M_L = \pm1$) ground term and $^4A_{2g}$ ($M_L = 0$) term. When spin-orbit coupling is switched on, each term splits into Kramers doublets.[26] Another issue relates to the magnetic couplings between Co^{2+} ions. Nearest-neighbour (NN) superexchange pathways within a kagome layer are depicted in Fig. S2, ESI†. There are two possible superexchange pathways involving either a μ_3-O(H) or a μ_2-O site with Co-O-Co angles of 99,13(4)° and 85,5(2)°, respectively. According to the Goodenough-Kanamori-Anderson (GKA) rules,[27] close to 90° superexchange is ferromagnetic (F) and a switch from F to AF is expected for a significant deviation from 90° Co-O-Co geometry. Published neutron diffraction results for high-spin Co^{2+} oxide phases evidenced F interactions for Co-O-Co angles less than about 100°.[24,28] Recent theoretical studies for high-spin Co^{2+} ion in 90° Co-O-Co bonding geometry with pseudo-spin J_{eff} = 1/2 have suggested a more complex situation in which F anisotropic Kitaev interactions coexists with a Heisenberg coupling, that can be F or AF depending on the local electronic structure.[29,30] Further neighbours interactions could also play an important role, as suggested in $BaCu_3(VO_4)_2(OH)_2$.[31]

Finally, we turn to the effects of finite size on the magnetic properties. The computed crystallite sizes (Table S1, ESI†) correspond to crystallites consisting of 1.1×10^4 to 1.4×10^4 unit cells and 25 to 28 kagome layers stacked in the *c* direction. As mentioned before, the magnetic susceptibility above ≈ 10 K bears resemblance to those of many bulk oxide phases containing high-spin Co^{2+} ions in sixfold environment as well as to those of six-coordinated high-spin Co^{2+} complexes. The low temperature behaviour is however likely to be impacted by the nanostructuration. The marked increases in $\chi(T)$ and $\chi(T).T$ below 10 K could be due to finite size or surface effects. The rapid initial increase of the experimental M(H) curve at 2 K compared to Brillouin functions for J = 3/2 or 1/2 (Fig. S8, ESI†) is consistent with a superparamagnetic contribution that could originate from the smallest nanoparticles or from surface layers. We also noted that the first magnetic study of synthetic vesignieite $BaCu_3(VO_4)_2(OH)_2$, which was performed on a powder with crystallite size on the order of a few nm, revealed neither a magnetic order or a spin glass transition down to 2 K.[11] Further data collected for polycrystalline samples with much shaper PXRD reflections,[32] showed the same behaviour as in the nanosized sample in the Curie-Weiss regime (T > 150K), but evidenced a magnetic ordering at T_N = 9 K.

Conclusions

We have successfully elaborated a new simple synthetic route under ambient pressure to quantitatively produce morphologically homogeneous and highly crystalline NPs (9-25 nm) of the cobalt orthovanadate $BaCo_3(VO_4)_2(OH)_2$. Its layered-kagome structure is topologically related to those of $BaCu_3(VO_4)_2(OH)_2$[11,12] and $BaNi_3(VO_4)_2(OH)_2$.[13] In the case of $BaCo_3(VO_4)_2(OH)_2$, the nanostructuration does not affect the crystal structure even at the atomic scale. Considering the magnetic properties, the effective moment indicates a high-spin state with an orbital contribution for the Co^{2+} ions. Remarkably, the susceptibility increases with no ZFC-FC difference as the temperature decreases down to 2 K. At low temperature, the magnetic behaviour is most likely affected by finite-size effects. Further studies will be needed to better understand the magnetic properties of $BaCo_3(VO_4)_2(OH)_2$, especially considering that high-spin Co^{2+} compounds are currently very attractive candidates in the search for new quantum magnets with spin-orbit coupling.[33] In particular, it would be useful to develop new synthetic routes to elaborate large micrometer-sized powder samples that would permit to investigate the bulk magnetic properties. It could also be interesting to prepare NPs with smaller crystallite size in order to reveal a superparamagnetic behavior with ZFC/FC irreversibility and blocking temperature above 2 K. For potential applications in spintronics, for instance, low-dimensional magnetic systems will have to be scaled down the nanometer regime where, eventually, superparamagnetism and thermal excitations will reduce the stability of the bulk magnetic state.

Conflicts of interest

There are no conflicts to declare.

Acknowledgement

Nicolas Stéphant is gratefully acknowledged for performing SEM measurements. This work was supported in part by the French Agence Nationale de la Recherche Grant ANR-18-CE30-022. The authors acknowledge the use of TEM instrumentation provided by the National Facility ELECMI ICTS ("Division de Microscopia Electronica", Universidad de Cadiz, DME-UCA). LL acknowledges funding from the Andalusian regional government (FEDER-UCA-18-106613), the European Union's Horizon 2020 research and innovation program (grant agreement 823717 – ESTEEM3) and the Spanish Ministerio de Economia y Competitividad (PID2019-107578GA-I00).

Notes and references

1 D. S. Inosov, *Adv. Phys.*, 2018, **67**, 149–252.
2 J. R. Chamorro, T. M. McQueen and T. T. Tran, *Chem. Rev.*, 2021, **121**, 2898–2934.
3 B. Huang, G. Clark, E. Navarro-Moratalla, D. R. Klein, R. Cheng, K. L. Seyler, D. Zhong, E. Schmidgall, M. A. McGuire, D. H. Cobden, W. Yao, D. Xiao, P. Jarillo-Herrero and X. Xu, *Nature*, 2017, **546**, 270–273.
4 Y. Lai, Z. Song, Y. Wan, M. Xue, C. Wang, Y. Ye, L. Dai, Z. Zhang, W. Yang, H. Du and J. Yang, *Nanoscale*, 2019, **11**, 5163–5170.
5 X. Zhang, Y. Xu, R. Zhong, R. J. Cava, N. Drichko and N. P. Armitage, *https://arxiv.org/abs/2106.13418*.
6 E. Y. Vedmedenko, R. K. Kawakami, D. D. Sheka, P. Gambardella, A. Kirilyuk, A. Hirohata, C. Binek, O. Chubykalo-Fesenko, S. Sanvito, B. J. Kirby, J. Grollier, K. Everschor-Sitte, T. Kampfrath, C.-Y. You and A. Berger, *J. Phys. Appl. Phys.*, 2020, **53**, 453001.
7 Y. Tokura, M. Kawasaki and N. Nagaosa, *Nat. Phys.*, 2017, **13**, 1056–1068.
8 C. Wellm, W. Roscher, J. Zeisner, A. Alfonsov, R. Zhong, R. J. Cava, A. Savoyant, R. Hayn, J. van den Brink, B. Büchner, O. Janson and V. Kataev, *https://arxiv.org/abs/2106.02437*.
9 R. Zhong, S. Guo, G. Xu, Z. Xu and R. J. Cava, *Proc. Natl. Acad. Sci.*, 2019, **116**, 14505.
10 T. Dordević and L. Karanović, *Acta Crystallogr. Sect. C*, 2013, **69**, 114–118.
11 Y. Okamoto, H. Yoshida and Z. Hiroi, *J. Phys. Soc. Jpn.*, 2009, **78**, 033701.
12 D. Boldrin, K. Knight and A. S. Wills, *J. Mater. Chem. C*, 2016, **4**, 10315–10322.
13 D. E. Freedman, R. Chisnell, T. M. McQueen, Y. S. Lee, C. Payen and D. G. Nocera, *Chem. Commun.*, 2012, **48**, 64–66.
14 R. L. Frost, S. J. Palmer, J. Čejka, J. Sejkora, J. Plášil, S. Bahfenne and E. C. Keeffe, *J. Raman Spectrosc.*, 2011, **42**, 1701–1710.
15 G. Busca, G. Ricchiardi, D. S. H. Sam and J.-C. Volta, *J. Chem. Soc. Faraday Trans.*, 1994, **90**, 1161–1170.
16 M. H. Kuok, S. C. Lee, S. H. Tang, M. Midorikawa and Y. Ishibashi, *Solid State Commun.*, 1988, **66**, 1035–1037.
17 G. Busca, *J. Raman Spectrosc.*, 2002, **33**, 348–358.
18 F. E. Mabbs and D. J. Machin, *Magnetism and Transition Metal*, Chapman and Hall: London, 1973.
19 R. Rawl, M. Lee, E. S. Choi, G. Li, K. W. Chen, R. Baumbach, C. R. dela Cruz, J. Ma and H. D. Zhou, *Phys. Rev. B*, 2017, **95**, 174438.
20 G. Nakayama, S. Hara, H. Sato, Y. Narumi and H. Nojiri, *J. Phys. Condens. Matter*, 2013, **25**, 116003.
21 Y. Shirata, H. Tanaka, A. Matsuo and K. Kindo, *Phys. Rev. Lett.*, 2012, **108**, 057205.
22 Y. Cui, J. Dai, P. Zhou, P. S. Wang, T. R. Li, W. H. Song, J. C. Wang, L. Ma, Z. Zhang, S. Y. Li, G. M. Luke, B. Normand, T. Xiang and W. Yu, *Phys. Rev. Mater.*, 2018, **2**, 044403.
23 F. Lloret, M. Julve, J. Cano, R. Ruiz-García and E. Pardo, *Inorganica Chim. Acta*, 2008, **361**, 3432–3445.
24 L. D. Sanjeewa, V. O. Garlea, R. S. Fishman, M. A. McGuire, J. Xing, H. Cao, J. W. Kolis and A. S. Sefat, *Inorg. Chem.*, 2020, **59**, 1029–1037.
25 L. D. Sanjeewa, V. O. Garlea, M. A. McGuire, C. D. McMillen and J. W. Kolis, *Inorg. Chem.*, 2019, **58**, 2813–2821.
26 R. Boča, *Coord. Chem. Rev.*, 2004, **248**, 757–815.
27 J. B. Goodenough, *Magnetism and the Chemical Bond, New York*, Interscience Publishers., 1963.
28 O. Mentre, F. Bouree, J. Rodriguez-Carvajal, A. El Jazouli, N. El Khayati and E. M. Ketatni, *J. Phys. Condens. Matter*, 2008, **20**, 415211.
29 H. Liu and G. Khaliullin, *Phys. Rev. B*, 2018, **97**, 014407.
30 R. Sano, Y. Kato and Y. Motome, *Phys. Rev. B*, 2018, **97**, 014408.
31 D. Boldrin, B. Fåk, E. Canévet, J. Ollivier, H. C. Walker, P. Manuel, D. D. Khalyavin and A. S. Wills, *Phys. Rev. Lett.*, 2018, **121**, 107203.
32 M. Yoshida, Y. Okamoto, M. Takigawa and Z. Hiroi, *J. Phys. Soc. Jpn.*, 2013, **82**, 013702.
33 C. M. Morris, N. Desai, J. Viirok, D. Hüvonen, U. Nagel, T. Rõõm, J. W. Krizan, R. J. Cava, T. M. McQueen, S. M. Koohpayeh, R. K. Kaul and N. P. Armitage, *Nat. Phys.*, 2021, **17**, 832–836.